review 1

by Minerals 27-------80 Paper

Submission date: 11-Dec-2023 03:27PM (UTC+0500)
Submission ID: 2255463357
File name: minerals-2781980-peer-review-v1.pdf (12.63M)
Word count: 7765
Character count: 40903

minerals

MDPI

Article

The Mechanism of Mineral Dissolution on the Development of Red Bed Landslides in the Wudongde Reservoir Region

YE Chenglin [1], SHI Yan [2], ZHAO Siyuan [1], LI Hua [1] and DENG Jianhui [1,*]

[1] College of Water Resource & Hydropower Sichuan University, No.24 South Section 1, Yihuan Road, Chengdu, 610065, China
[2] THREE GORGES GEOTECHNICAL ENGINEERING CO.LTD. , China
* Correspondence: jhdeng@scu.edu.cn; Tel.13980959251:

Abstract: The Wudongde reservoir region exhibits a notable prevalence of landslides within the red bed reservoir stratum. In this study, we delve into the impact of mineral dissolution on the development of red bed landslides in the reservoir region by utilizing the Xiaochatou landslide as a representative case study. Considering the inherent susceptibility of red bed formations to erosion, collapse, and softening when exposed to water, an investigation is conducted to examine the consequences of mineral dissolution on landslides occurring in these areas. To initiate the study, mineral analysis and identification were performed on rock samples obtained from the Xiaochatou landslide site, which unveiled a rock structure primarily comprising alternating layers of sandstone and mudstone. Subsequently, we subjected sandstone and conglomerate specimens to immersion in deionized water. To further investigate the effects of immersion in water, advanced techniques such as scanning electron microscopy (SEM), ion chromatography (IC), and inductively coupled plasma (ICP) analysis were employed. These techniques allow for a detailed examination of the microstructure of the rock mass and the assessment of dissolved ion concentrations at different stages of immersion. Furthermore, we elucidated the intricate mechanism of gypsum dissolution during the soaking process by utilizing the hydrogeochemical simulation software PHREEQC. Our findings reveal that sandstone and conglomerates harbor a notable quantity of gypsum, which readily dissolves in water. Prolonged immersion leads to erosion cavities within the sandstone, thereby augmenting its permeability. The concentration of SO_4^{2-} ions in the soaking solution emerges as the highest, followed by Ca^{2+} and Na^{+}. The notable significance is the dissolution of gypsum, whose intricate mechanism is contingent upon diverse environmental conditions. Variations in ion concentration profoundly influence the saturation index (SI) value, with the pH value playing a crucial role in shifting the reaction equilibrium. Regarding the deformation mode of the landslide, it manifests as a combination of sliding compression and tension cracking. The fracture surface of the landslide assumes a step-like configuration. As the deformation progresses, the mudstone layer takes control over the sliding process, causing the sandstone to develop internally narrow-top and wide-bottom cracks, which propagate upward until the stability of the slope rock mass is compromised, resulting in its rupture. It is expected to provide suggestions to prevent and reduce geological and engineering disasters in the red bed area.

Keywords: red bed landslide; mineral composition; microstructure; hydrochemistry simulation; Mechanism of water-rock reaction

Citation: To be added by editorial staff during production.

Academic Editor: Firstname Lastname

Received: date
Revised: date
Accepted: date
Published: date

Copyright: © 2023 by the authors. It was submitted for possible open access publication under the terms and conditions of the Creative Commons Attribution (CC BY) license (https://creativecommons.org/licenses/by/4.0/).

1. Introduction

The red beds in China can be categorized into several types, including the southwest red beds, dominated by Sichuan-Yunnan red beds; northwest red beds, dominated by

Gansu red beds; central and southeast red beds; and other red beds, dominated by Tibet red beds [1-3].

The red bed in the Jinsha River, an essential part of the Sichuan-Yunnan red bed strata, has garnered the attention of researchers due to the construction of cascade hydropower stations in the river's lower reaches. Due to its unique engineering properties, the red bed area often experiences geological disasters like landslides. The Wudongde reservoir area, particularly, is characterized by a high incidence of red bed landslides and is associated with a large-scale landslide river-blocking event in history. Therefore, it is crucial to study these landslides [4,5].

The Sichuan Basin and the Three Gorges Reservoir area in China are characterized by the prevalence of red bed strata, commonly called "landslide-prone strata" [6]. Red bed strata are terrestrial sedimentary formations characterized by alternating layers of red mudstone and sandstone [7]. These landslides are commonly initiated by precipitation and occur along the planes of stratification. A notable instance is the torrential rainfall experienced on July 9 and 10, 1989, surpassing 200 mm across the majority of the Sichuan Basin. This event instigated over 10,000 landslides, predominantly comprising bedding plane landslides [8]. Under the influence of groundwater infiltration, the presence of weak interlayers undergoes a process of softening upon encountering water, subsequently developing into slip zones [9]. The underlying reasons for this phenomenon, which involves unique hydro-mechanical interactions, are closely associated with the type of rock mass, its structural characteristics, and the content of hydrophilic minerals such as clay minerals [10]. The dissolution characteristics of gypsum-bearing red layers have received significant attention. When these red layers come into contact with water, gypsum undergoes extensive dissolution, resulting in mineral loss within the rock mass. This process leads to an increase in porosity and enhanced permeability. The dissolution phenomenon is particularly pronounced in acidic environments [11,12].

[13,14] meticulously elucidates the intricate features of black strata weathering through a comprehensive analysis encompassing chemical, mineralogical, and hydrological considerations. Moreover, they succinctly expound upon the underlying mechanisms that give rise to disastrous consequences. The saturation index (SI) serves as a valuable metric for assessing the intricate interplay between water and rock, making it an indispensable tool for analyzing the dynamic nature of their interaction [15]. The utilization of the PHREEQC simulation software for chemical reactive transport processes during water-rock reactions has yielded promising results. The simulations have demonstrated the software's capability to effectively model and simulate the intricate geochemical reactions that occur under relatively simple chemical transport conditions. This success highlights the utility of PHREEQC as a powerful tool for studying and understanding complex water-rock interactions [16,17].

In this paper, the Xiaochatou landslide in the Wudongde reservoir area serves as a case study. Through comprehensive field geological surveys, the focus of the study lies in investigating the specific characteristics of water-rock interaction within the red-bed soft rock formation. Furthermore, an in-depth analysis of the instability mechanism of red-bed

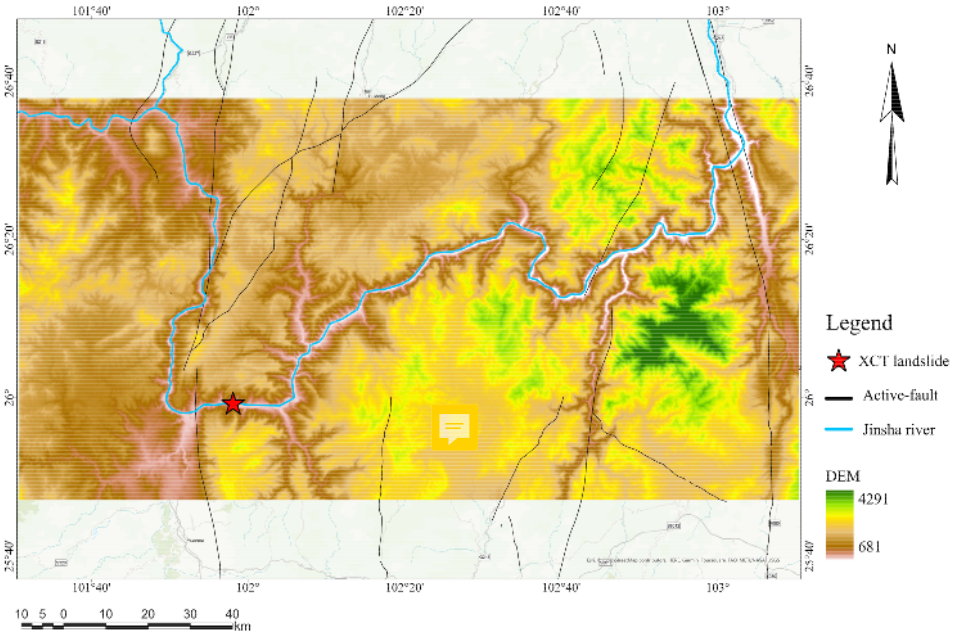
landslides under the influence of hydrochemical action is conducted. The research findings contribute significantly to the prevention and mitigation of geological disasters in the reservoir area. Consequently, they play a crucial role in ensuring the secure and stable operation of the reservoir area, thereby safeguarding the surrounding environment and communities.

2. Site description

The Xiaochatou landslide (Figure 1) is located on the right bank of the Jinsha River, approximately 2 km upstream of Malamo village, 98.3 km downstream of the Wudongde dam site, and 13.6 km upstream of Longchuan riverside town. The front edge of this landslide is close to the Jinsha River, at an elevation of around 1300 m. A gully has developed on both sides of the boundary. The maximum width of the front edge is about 570 m, which gradually decreases to 300 m, and its longitudinal length is approximately 700 m. The plane area is approximately 0.29 km^2. The thickness of the front edge and the trailing edge is 50-60 m, and the middle part is 110-120 m. Its volume is around 2,400 × 10^4 m^3. The landform of this landslide area is gentle on the top and steep on the bottom, with an average gradient of 26° to 40°. A vertical ridge is about 30 m high at the trailing edge. The landslide body has a three-scale platform, with the 1080-1090 m elevation platform being approximately 30 m wide. The front edge is slightly upturned. Saggy terrain with banded distribution is located on the side of this landslide. The surface layer of this landslide is gravel soil containing gypsum debris, the middle layer is a thick block, and the bottom is mainly rock fragments. The underlying bed is sandstone, siltstone, and silty mudstone of the Cretaceous Matoushan Formation and Jiangdihe Formation. The Jiangdihe Formation contains gypsum lenses, and the rock layer tends to be northeast, with an inclination angle of 10° to 16°.



(a)



(**b**)

Figure 1. (a) The Xiaochatou landslide exhibits a distinctive landscape characterized by significant geological deformations and topographical alterations. (b) The study region, encompassing the Xiaochatou landslide, is located in a specific geographic location. It is typically described in terms of its geographical coordinates or by referencing nearby landmarks or boundaries. The location may be indicated using latitude and longitude coordinates or by specifying the regional relation to cities, or geographical features.

3. The characteristics of the reaction of water-rock in red-bed rock

The red rock samples collected from the Xiaochatou landslide include conglomerate, sandstone, mudstone, calcareous cement, and soil samples from the bottom layer. The complete conglomerate rock and sandstone were prepared as cylindrical samples with a diameter of Φ50mm and a height of 100mm. Due to transportation constraints, the mudstone samples were small and were ready as cylindrical samples with a diameter of Φ25mm and a height of 50mm.

3.1 Mineral analysis and identification

The mineral composition and proportion of the red-bed rock (soil) sample obtained by X-ray diffractometer (XRD) are shown in Table 1. The photos of XCT-0 and XCT-0′ rock samples under the polarizing microscope are shown in Figure 2. The identification results of rock samples are as follows:

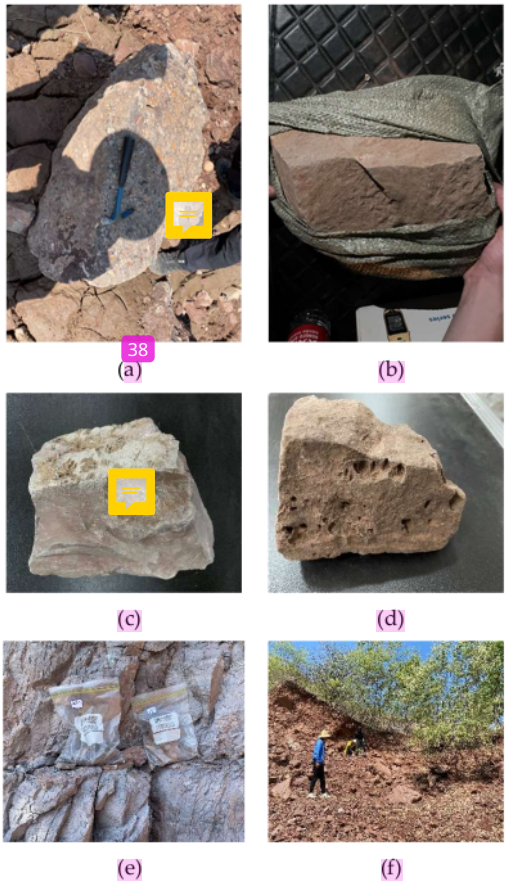


Figure 2. Landslide red bed samples. (a) Conglomerate XCT-0 (b) Sandstone XCT-0′. (c) Mudstone XCT-3. (d) Dissolved sandstone XCT-2′′. (e) Calcium deposits XCT-2&2′. (f) Soil under pebbles XCT-3.

Table 1. XRD mineral composition of red-bed rock samples

Sample	Quartz	Calcite	Dolomite	Feldspar	Gypsum	Muscovite	Chlorite
XCT-0	37	12	34	8	8		1
XCT-0′	52	20		13	10	4	1
XCT-1	84	10		6			
XCT-2	7	93					
XCT-2′	6	7			87		
XCT-2′′	42	18				40	
XCT-3	30	18	36				16

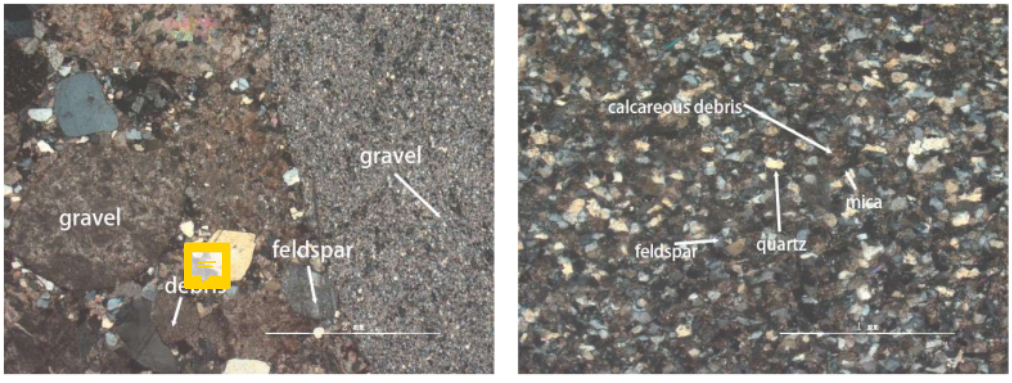
[1] The number in the table represents the percentage.

The rock sample XCT-0 is a calcareous sand conglomerate composed of several gravels and mixed interstitial materials. The gravels range from 2mm to 50mm, mostly round and sub-round shapes and good roundness. The composition of the conglomerate is diverse and includes four main types: (metamorphic) sandstone gravel, quartz-schist

gravel, dolomite gravel, and andesite-basalt gravel. The interstitial materials are distributed among the gravel particles. The components include rock debris, quartz, feldspar, calcium, and iron-rich sediment. These include rock fragments, mostly between 0.152mm in size, with a composition similar to gravel. The particle size of quartz and feldspar is between 0.051mm. The quartz is primarily clear, while the feldspar is altered and cloudy. Calcite is present as granular particles with a particle size below 0.6mm. These particles exhibit advanced white interference color and are stained red by the alizarin red reagent. The iron-rich sediment appears reddish-brown dust mixed with rock debris between the sandy components.

Sample XCT-0′ is a fine-grained, calcareous sandstone composed of feldspar, quartz, and a significant amount of interstitial material (Figure 3). Debris in this sample is mostly angular to sub-angular. Particle sizes range primarily between 0.05 and 0.2mm. The particles have poor roundness but good sorting. Most particles are in point-to-line contact. Debris consists primarily of quartz, feldspar, mica, and trace amounts of chlorite. The quartz in this sample is colorless with low protrusions and has a gray and gray-white interference color. The surface is unaltered and clean. The feldspar and double crystal characteristics development. Feldspar crystals exhibit dual characteristics, and both alkaline feldspar and plagioclase are visible. The surface is more turbid due to alteration. Mica, biotite, and muscovite are visible, mixed between felsic particles, and distribution is directional. Chlorite has a green-light-green interference color, often covered by its color or an abnormal interference color. Interstitial material is distributed between debris particles in a filling shape, and the components are primarily calcareous with trace amounts of siliceous and iron-muddy material. The calcium in this sample exhibits an advanced white interference color and foams when exposed to dilute hydrochloric acid, indicating the presence of calcite. The siliceous material is finely grained. The iron-muddy material is yellowish-brown to black-brown and reddish-brown, mainly in a granular form [18].

This section may be divided by subheadings. It should provide a concise and precise description of the experimental results, their interpretation, as well as the experimental conclusions that can be drawn.



(a) (b)

Figure 3. Polarizing Microscope Photos of rock samples: (a) Polarizing Microscope Photos of XCT-0 (b) Polarizing Microscope Photos of XCT-0′

3.2 Water immersion dissolution test

3.2.1 The variation characteristics of solution ion concentration during the dissolution process

In this dissolution study, five standard cylindrical samples of conglomerate and sandstone were weighed for their natural and oven-dried masses and placed in an empty container [2,3]. Subsequently, 1000 mL of deionized water was added to each sample. After 7, 14, 21, and 28 days, 10 mL of the soaking solution's supernatant was collected. The concentrations of cations and anions in the dissolved solution were quantitatively analyzed using inductively coupled plasma emission spectrometry (ICP) and ion chromatography (IC). The result shows in Figure 4.

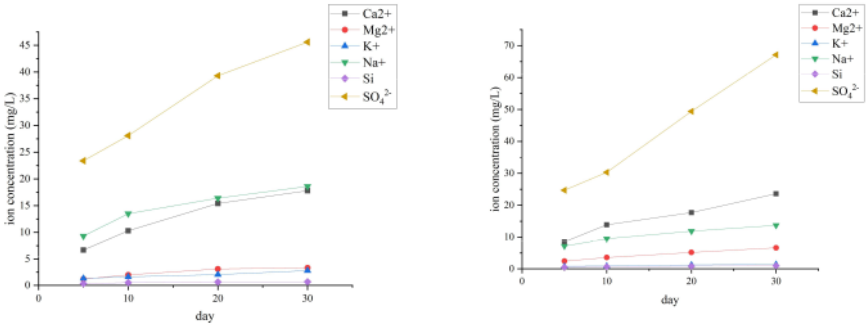


Figure 4. Variation curve of ion concentration with time after immersion of rock samples. (a) Variation curve of ion concentration with time after immersion of conglomerate. (b) Variation curve of ion concentration with time after immersion of sandstone.

Indicates that the SO_4^{2-} concentration is highest in the soak solution of conglomerate, and the highest cation concentrations are Na^+ followed by Ca^{2+}. The SO_4^{2-} concentration had the highest rate of increase, followed by Ca^{2+} and Na^+. Concentrations of other ions remained relatively stable. Similarly, the SO_4^{2-} concentration is highest in the immersion solution of sandstone, and the highest cation concentrations are Ca^{2+}, followed by Na^+ and Mg^{2+}. The SO_4^{2-} concentration had the highest rate of increase, followed by Ca^{2+} and Na^+. Concentrations of other ions remained relatively stable.

The mineral analysis revealed that the soluble minerals in conglomerate and sandstone consist primarily of gypsum, calcareous cement, and chlorite. Due to the high concentration of Ca^{2+} and SO_4^{2-} in the deionized water used in this analysis, gypsum is the primary mineral that dissolves. Gypsum is a soluble sedimentary rock commonly found in Salt Lake deposits. It has a chemical formula of $CaSO_4{\cdot}2H_2O$ and belongs to the monoclinic crystal system [19]. Gypsum crystals are predominantly platy, compact, and fibrous and are more frequently found in red sandstone and shale. The following reaction can represent the hydrolysis of gypsum:

$$CaSO_4 \cdot 2H_2O \rightleftharpoons Ca^{2+} + SO_4^{2-} + H_2O \quad (1)$$

The gypsum in the red-bed rock mass of the reservoir area dissolves in groundwater and is collected in rock cracks and bedding by water flow, as shown in Figure 5a. As the solution concentration increases, the gypsum precipitates in crystal form once it reaches dissolution equilibrium. The precipitated gypsum adheres to the rock mass surface or fills cracks between the original rock mass due to losing the gypsum mineral component in the original rock mass. This process destroys the structure of the red-bed rock mass, forming some dissolution holes, as shown in Figure 5b. This increases the porosity and enhances the permeability.



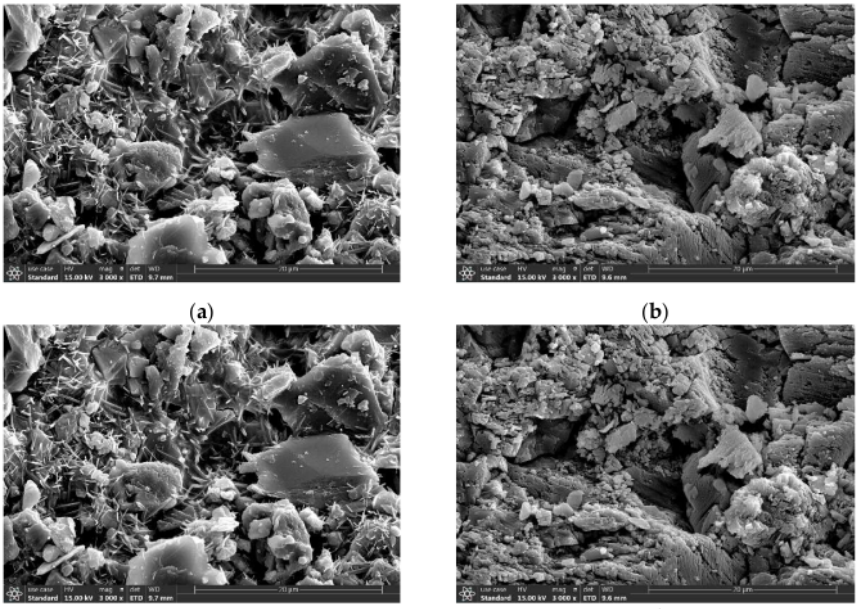
(**a**) (**b**)

Figure 5. Red bed soft rock containing gypsum. (a) Gypsum layer filled in conglomerate cracks. (b) Dissolution cavities in conglomerate.

3.2.2 The microstructure characteristics before and after immersion

In Figure 6a, a substantial quantity of fibrous and elongated gypsum cement is prominently dispersed across the surface of the rock mass specimen. Meanwhile, Figure 6c portrays the presence of chlorite crystals exhibiting a honeycomb-like configuration, reminiscent of delicate leaves adorned with slender hexagonal blades or plates. Prior to immersion, microscopic examination of these crystals reveals predominantly blocky and plate-like structures, characterized by smooth and level crystal planes, interconnected networks exhibiting close proximity, remarkable structural integrity, a limited presence of adhered clay minerals, and an absence of discernible signs of corrosion damage.

Figures 6b and 6d illustrate the alteration in the microscopic morphology of the rock sample subsequent to the soaking process, primarily attributed to water flow dissolution. The rock block undergoes fragmentation, resulting in the formation of smaller fragments, accompanied by distinct dissolution marks resembling knife-like incisions on the surface. Moreover, the overall integrity of the rock mass diminishes noticeably. Soluble minerals present in the rock, such as gypsum and chlorite, undergo dissolution and hydrolysis, giving rise to numerous dissolved pores. These dissolved pores significantly augment the contact area between the rock and water, facilitating further dissolution within the interior of the rock. Consequently, this dissolution process leads to the generation of fine particles as a product.

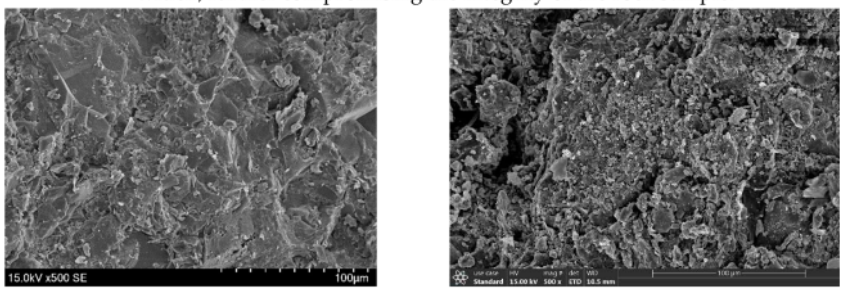


(**a**) (**b**)

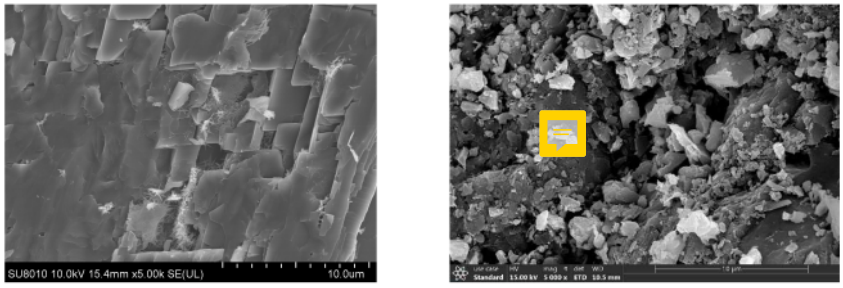
(**c**) (**d**)

Figure 6. Microstructure at different magnifications before and after immersion. (a) Microstructure before immersion (3000×). (b) Microstructure after immersion (3000×). (c) Microstructure before immersion (5000×). (d) Microstructure after immersion (5000×).

Figures 7a and 7c depict the initial state of the rock samples prior to immersion, showcasing stepped surfaces and sporadic distribution of gypsum. The crystals predominantly exhibit plate-like and elongated strip structures, with a few discernible small cracks. In contrast, Figures 7b and 7d provide a scence into the altered microscopic morphology of the rock sample subsequent to the dissolution of gypsum minerals in deionized water, resulting in the formation of dissolution holes. The fine particles present on the surface undergo either exfoliation or dissolution, leading to a rough and loosely structured arrangement of the crystal planes. Following the dissolution process, the structure assumes a flaky configuration, while the micro-cracks gradually extend and widen, further compromising the integrity of the rock sample.



(**a**) (**b**)



(**c**) (**d**)

Figure 7. Microstructure at different magnifications before and after immersion. (a) Microstructure before immersion (3000×). (b) Microstructure after immersion (3000×). (c) Microstructure before immersion (5000×). (d) Microstructure after immersion (5000×).

4. Numerical analysis of dissolution effect for red beds

We conducted an equilibrium process simulation using the hydrogeochemical software PHREEQC, focusing on conglomerate and sandstone samples from the Xiaochatou landslide [16,20-23]. We simulated the dissolution and precipitation of red-bed minerals using the saturation index method [24-27].

4.1 Saturation index

The saturation index is a vital mineral parameter based on the principle of thermodynamics. According to the SI, we can determine the reaction state between water and minerals [28].

For the reaction:

$$aA + bB = cC + dD \quad (2)$$

The AP (activity product) is expressed as:

$$AP = [C]^c[D]^d/[A]^a[B]^b \quad (3)$$

If all components are ions, they can be represented by IAP. When the reaction reaches equilibrium, we assume there are a′ mol A, b′ mol B, c′ mol C, and d′ mol D. According to the law of mass action, the activity product K is as follows:

$$K = [C]^{c'}[D]^{d'}/[A]^{a'}[B]^{b'} \quad (4)$$

The expression of saturation index SI is:

$$SI = \lg\frac{IAP}{K} \quad (5)$$

The mineral is saturated or supersaturated when SI is 0 or greater than 0. This mineral will tend to stop dissolving or even precipitate. When SI is less than 0, the mineral is unsaturated in groundwater. When it still exists in the water environment, it will tend to dissolve and gradually become saturated.

When the Saturation Index (SI) of a mineral is 0 or greater than 0, it indicates that the mineral is either saturated or supersaturated in the given environment. In such a state, the

mineral is prone to cease dissolving or even precipitate out of the solution. The presence of excess minerals beyond saturation levels promotes the formation of solid precipitates.

Conversely, when the SI is less than 0, it signifies that the mineral is unsaturated in the groundwater. In this scenario, if the mineral persists in the water environment, it will tend to dissolve gradually. Over time, as dissolution continues, the mineral concentration in the water may increase, eventually reaching a point of saturation.

4.2 The simulation of the process of dissolution

The saturation index method calculates the dissolution of red bed minerals, and the dissolution and precipitation state of red bed conglomerate and sandstone minerals components in such an environmental aqueous solution can be determined. This way, we can predict the chemical weathering trend of the red bed. This paper mainly analyzes the variation of SI of these rock-forming minerals, which greatly influence rock mass structure, such as Albite, Gypsum, K-mica, Illite, and Kaolinite. Table 2 shows the ion concentration analysis results of samples in the layer area.

Table 2. Water quality analysis unit: mg/L

Rock sample	Time(day)	Al	Ca^{2+}	Mg^{2+}	K^{+}	Na^{+}	Si	SO_4^{2-}
conglomerate	5	0.04	6.70	1.19	1.32	9.30	0.34	23.4
	10	0.03	10.30	1.99	1.63	13.50	0.52	28.1
	20	0.04	15.4	3.12	2.06	16.4	0.650	39.3
	30	0.03	17.8	3.33	2.81	18.6	0.688	45.6
sandstone	5	0.07	8.54	2.43	0.83	7.19	0.51	24.7
	10	0.05	13.90	3.58	0.92	9.52	0.69	30.3
	20	0.07	17.7	5.21	1.24	11.9	0.859	49.4
	30	0.06	23.6	6.67	1.40	13.7	0.978	67.1

This paper uses the PHREEQC compiled by the United States Geological Survey (USGS) to analyze the above water samples. To obtain the SI value that can better reflect the actual water-rock interaction state, the calculation method of this software is as follows: First of all, the various forms of dissolution groups in the water-rock system are solved. Then, the concentration of free ions is obtained by calculating various complexes. In this step, it can also calibrate the ionic strength and determine ion activity more accurately. Finally, the SI value is obtained [15,29]. The conditions of water samples (temperature, pH, ion concentration, et al.) are input into the PHREEQC. The thermodynamic database automatically installed with PHREEQC can establish the corresponding equations. The equations are solved by the Newton-Raphson iteration method. Considering the influence of the complex, the SI value of each mineral in the water sample is finally calculated.

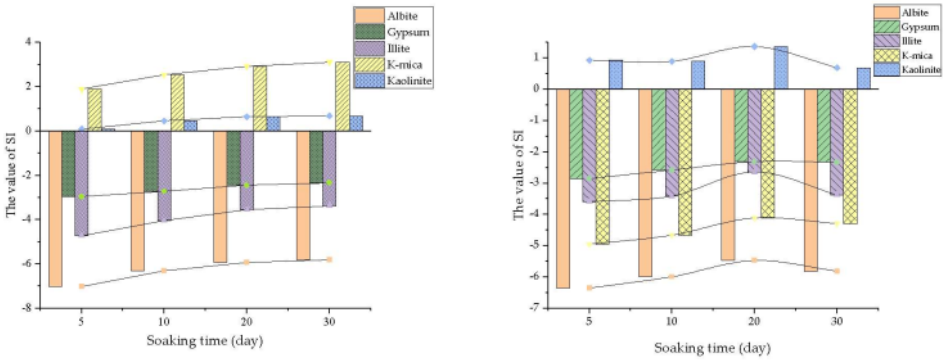


Figure 8. (a) Trend chart of SI of the conglomerate sample with soaking time. (b)Trend chart of SI of sandstone sample with soaking time.

Based on the observations presented in Figure 8, it is evident that the Saturation Index (SI) values for Kaolinite and K-mica consistently exceed 0 in both the conglomerate and sandstone samples. On the other hand, the SI values for the other minerals in the conglomerate sample remain below 0. Similarly, in the sandstone sample, only Kaolinite demonstrates an SI value above 0.

These findings suggest that Illite, Gypsum, and Albite do not separate or precipitate out in the conglomerate samples. Instead, minerals such as Kaolinite and K-mica gradually undergo precipitation over time. In contrast, the sandstone sample exhibits a different pattern. Throughout the entire process, only Kaolinite is observed to precipitate, while the other minerals do not exhibit significant changes in their SI values.

These observations provide valuable insights into the mineralogical behavior within the conglomerate and sandstone samples, highlighting the selective precipitation of specific minerals over others under the given conditions.

4.3 The sensitivity analysis of mineral dissolution and precipitation

Interestingly, certain environmental conditions play a significant role in the process of dissolution and precipitation. Therefore, it is imperative to conduct sensitivity analysis on various parameters during numerical analysis [30-32].

Sensitivity analysis serves several purposes in research. Firstly, it helps identify the most critical parameters that significantly affect the model's output. This understanding is crucial for focusing resources and efforts on the most influential factors. Secondly, sensitivity analysis allows us to assess how different combinations of parameters impact the model's output process, providing insights into complex interactions and potential synergies or trade-offs. Lastly, sensitivity analysis helps identify parameters that have minimal impact on the model's output, allowing for a reduction in computational burden and uncertainty associated with those parameters.

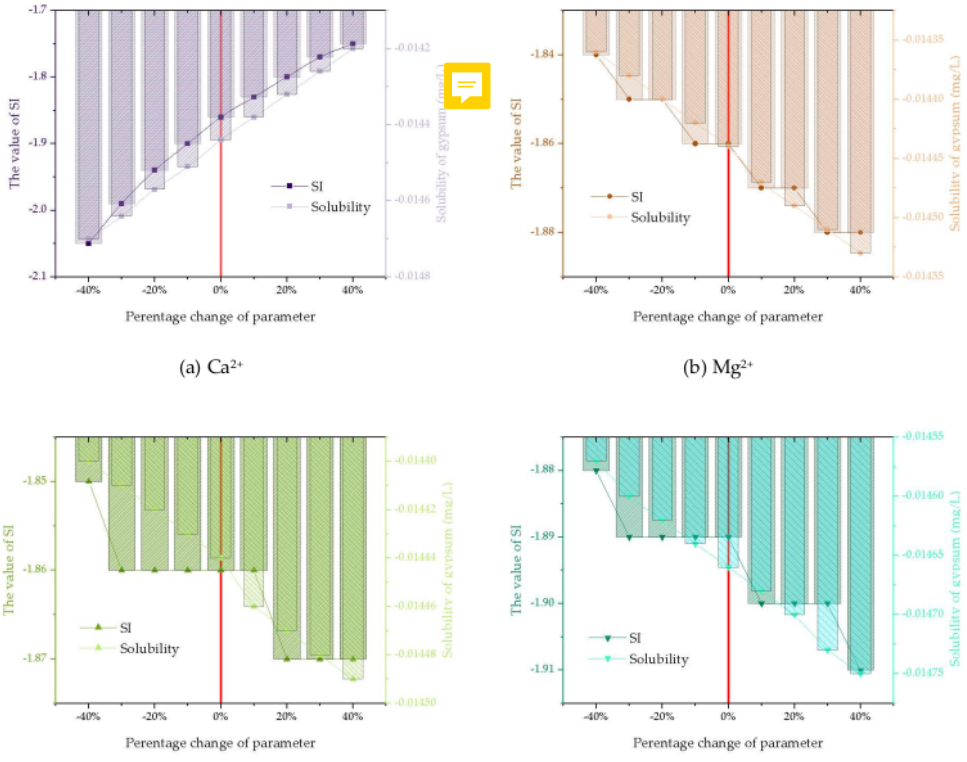
In the referenced paper, the dissolution and precipitation of gypsum are recognized as playing a prominent role in the Xiaochatou landslide [33-36]. Consequently, the paper conducts a sensitivity analysis specifically focused on the dissolution of gypsum in water

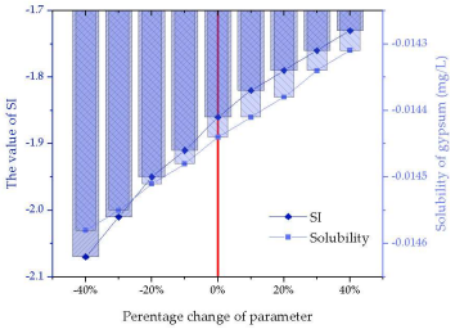
samples obtained from the Jinsha River. The results of the water quality analysis, including the relevant data, are presented in Table 3. These findings are crucial for understanding the behavior of gypsum in the context of the landslide and contribute to a comprehensive understanding of the factors influencing the landslide dynamics.

Table 3. Water quality analysis of JSJ-1 unit: mg/L

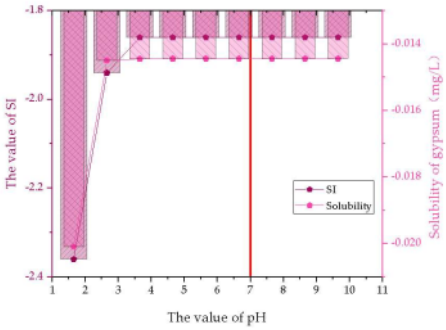
Sample	Ca^{2-}	Mg^{2+}	K^{+}	Na^{+}	PO_4^{2-}	HCO_3^{-}	SO_4^{2-}	pH
JSJ-1	53.5	17.7	2.71	48.2	<3	184	62.9	7.65

Using the EQUILIBRIUM_PHASES in PHREEQC, some parameters were set as the environmental variables, and others remained unchanged [37]. We consider six parameters in this paper: the ion concentration of Ca^{2+}, Mg^{2+}, Na^{+}, HCO_3^{-}, SO_4^{2-}, and the value of pH. We assumed this dissolution process happened in 1 kg of JSJ-1 water sample. The dissolution and precipitation capacity of minerals is characterized by the amount of minerals dissolved and liberated and the value of SI during the dissolution equilibrium. Figure 9 plots the results on the graph.

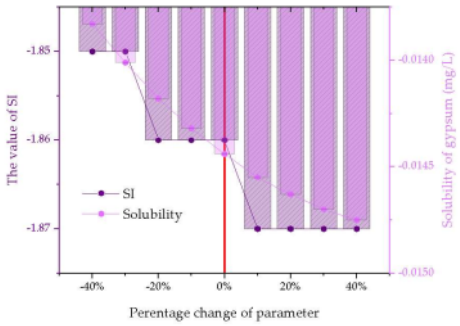




(e)SO_4^{2-}



(f) pH



(g) SUM

Figure 9. The curve of dissolution and precipitation ability of gypsum with different parameters change. Figure 9 (g) plot shows the superposition process of the above parameters.

Then, sensitivity analysis was performed [38-41]. In this paper, the sensitivity function is used to evaluate gypsum dissolution. The sensitivity function can be available in closed form or given only as a numerical procedure to compute y given by x. Typically, the output y is a scalar variable that "summarizes" the wide range of variables (often time series, possibly spatially distributed) provided by the simulation. The sensitivity function of each parameter can be obtained from Figure 9 by the least square method. To rank the influence of each parameter, the sensitivity indices that the sensitivity function can define are often employed in sensitivity analysis and importance measures. These synthetic indices quantify the relative contribution to output uncertainty from each input. A sensitivity index of zero means that the associated information is non-influential, while the higher the index, the more influential the intake. In this case, the slope of the linear fitting of each parameter and the range of change is considered to such sensitivity index. The sensitivity ranking of each parameter can be given in Table 4. The sensitivity ranking from large to minor is SO_4^{2-}, pH, Ca^{2+}, Mg^{2+}, HCO^{3-}, and Na^{+}.

Table 4. The sensitivity function and sensitivity index of each parameter

parameter	function	index
Ca^{2+}	y=0.36x-1.87	0.36
Mg^{2+}	y=-0.05x-1.86	0.05
Na^{+}	y=-0.02x-1.86	0.02
HCO_3^-	y=-0.03x-1.89	0.03
SO_4^{2-}	y=0.42x-1.87	0.42
pH	y=0.4x-2.13	0.40
SUM	y=-0.03x-1.86	0.03

5. Discussion

The water immersion test results indicate that sandstone is more susceptible to dissolution by water [42]. Additionally, the experiment on the wave velocity of mudstone during the dry-wet process reveals that the strength attenuation of mudstone is significantly reduced [43,44]. Furthermore, we examined the dissolution saturation of gypsum in the water of the Jinsha River. Based on the results above, we can draw the following discussions.

5.1 Discussion of the Numerical Analysis

The simulation of sandstone and conglomerate dissolution indicates that chemical weathering is a significant factor in forming cracks on the rock surface during dissolution [25]. Furthermore, by considering the changes in Ca^{2+} and SO_4^{2-} ion concentrations and SI values, we can conclude that gypsum is the primary dissolved substance during the dissolution process.

A qualitative analysis of gypsum dissolution is necessary. Nevertheless, the mechanism of how dissolution occurs under various environmental conditions is too complex to explain clearly. Therefore, we select some typical parameters for sensitivity analysis. While the equation for gypsum is suitable for interpreting the high sensitivity of SO_4^{2-} and Ca^{2+}, it cannot provide a reasonable explanation for the variation phenomenon when the concentrations of Mg^{2+}, HCO_3^-, and Na^+ change. The slight effect of changes in ion concentrations on the SI value can be explained by the pH value, which shifts the reaction equilibrium [24,29]. The pH and SI curves demonstrate that the SI value increases in an acidic environment but approaches 0 in a neutral environment. This explains the variation phenomenon when the concentrations of Mg^{2+}, HCO_3^-, and Na^+ change. The SUM plot illustrates the result when the above parameters change together. This figure demonstrates that the influence of each parameter on the dissolution effect is not simply additive, and explaining this reaction requires an understanding of the movement of reaction equilibrium. The dissolution of gypsum in rock samples predominantly contributes to the overall mineral depletion. It has varying sensitivity to changes in environmental parameters, resulting in decreased mechanical properties of rock samples.

5.2 Discussion of the mechanism of Xiaochatou landslide

The red layer landslide in the reservoir area consists of thick sandstone interbedded with thin mudstone. The sandstone, characterized as hard rock, contains gravel at its base,

while the mudstone is classified as soft rock [9,29,45,46]. The sandstone, which contains soluble minerals such as gypsum, is highly permeable and acts as an aquifer, while the mudstone is impermeable. Water infiltrating from the ancient landslide-dammed lake dissolves gypsum, clay minerals, and calcium cementation in the sandstone, which are carried away by water flow, forming numerous dissolution pores that further enhance permeability. Tensile cracks perpendicular to the sliding surface form inside the sandstone near the locking or misalignment points of the sliding surface due to the concentration of tensile stress. Cracks facilitate surface water infiltration, which flows along the cracks and converges at the interface between sandstone and mudstone. The water further infiltrates the slope, softening the mudstone and reducing its strength. The upper sandstone fracture surface reforms and continuously expands upward.

6. Conclusion

(1) The sandstone conglomerates in the red beds of the Wudongde reservoir area contain soluble minerals such as gypsum and chlorite. When the rock samples are immersed in water, the dissolved ions are mainly SO_4^{2-}, Ca^{2+}, and Na^{+}, and the primary mineral dissolved is gypsum. The microstructure of the rock changes after immersion, with easily dissolved pores being generated, which increases the permeability of the rock mass.

(2) The dissolution of sandstone and conglomerate is affected by chemical weathering, which forms cracks on the rock surface. Gypsum is the primary substance dissolved during the process. The dissolution mechanism is intricate under diverse environmental conditions, and the effect of changes in ion concentration on the SI value is explained by the pH value that shifts the reaction equilibrium. The SUM plot shows that the impact of each parameter on the dissolution is not simply additive. Gypsum dissolution accounts for most of the total dissolution and decreases the mechanical properties of rock samples.

(3) The deformation pattern exhibited by the landslide entails the occurrence of slip-compression-induced tensile fractures within the low dip angle strata. Within this framework, the presence of water from the Jinsha River, permeating the mudstone and facilitating gypsum dissolution, assumes a pivotal role as the regulating layer for slip control. Consequently, the sandstone undergoes internal structural changes, characterized by the formation of vertically elongated fissures that exhibit a narrow apex and a broader base. Throughout the progressive deformation, these fissures persistently propagate and extend vertically until the stability threshold of the slope rock mass is surpassed, ultimately leading to its catastrophic collapse.

Author Contributions: Conceptualization, ZHAO Siyuan; Methodology, Chenglin YE; Software, ZHAO Siyuan; Investigation, Chenglin YE; Resources, LI Hua; Writing – original draft, Chenglin YE; Writing – review & editing, Chenglin YE; Supervision, SHI Yan and DENG Jianhui; Project administration, DENG Jianhui; Funding acquisition, LI Hua.

Funding: This research received no external funding

Data Availability Statement: The original contributions presented in the study are included in the article.

Acknowledgments:

Conflicts of Interest: The authors declare no conflict of interest.

References

1. Cheng, Q.I.; Kou, X.B.; Huang, S.B.; Zhou, Y.J. The distributes and geologic environment characteristics of red beds in China. *Journal of Engineering Geology* **2003**, *2004(1)*, 34-40.
2. Kruiver, P.P.; Dekkers, M.J.; Langereis, C.G. Secular variation in Permian red beds from Dôme de Barrot, SE France. *Earth Planetary Science Letters* **2000**, *179*, 205-217, doi:https://doi.org/10.1016/S0012-821X(00)00104-7.
3. Zhang, H.Z.; Liu, J.F. Microstructures, mineral compositions, and mechanical properties of red-layers in southern China. *Advances in Materials Science Engineering Fracture Mechanics* **2018**, *2018*, 1-9, doi:https://doi.org/10.1155/2018/9601386.
4. Wu, L.; Zhang, L.M.; Zhou, Y.; Xu, Q.; Yu, B.; Liu, G.; Bai, L. Theoretical analysis and model test for rainfall-induced shallow landslides in the red-bed area of Sichuan. *Bulletin of Engineering Geology the Environment* **2018**, *77*, 1343-1353.
5. Xu, Q.; Liu, H.X.; Ran, J.X.; Li, W.H.; Sun, X. Field monitoring of groundwater responses to heavy rainfalls and the early warning of the Kualiangzi landslide in Sichuan Basin, southwestern China. *Landslides* **2016**, *13*, 1555-1570, doi:https://doi.org/10.1007/s10346-016-0717-3.
6. Jian, W.X.; Wang, Z.J.; Yin, K.L. Mechanism of the Anlesi landslide in the three gorges reservoir, China. *Engineering Geology* **2009**, *108*, 86-95.
7. Gao, L.; Zhang, L.M.; Chen, H.X. Likely scenarios of natural terrain shallow slope failures on Hong Kong Island under extreme storms. *Natural Hazards Review* **2017**, *18*, B4015001, doi:https://doi.org/10.1061/(ASCE)NH.1527-6996.0000207.
8. Kong, J.M.; Chen, Z.S. The translational landslide in red stratum located in east Sichuan in July, 1989. Landslide column. **1989**.
9. Miao, H.B.; Wang, G.H.; Yin, K.L.; Kamai, T.; Li, Y.Y. Mechanism of the slow-moving landslides in Jurassic red-strata in the Three Gorges Reservoir, China. *Engineering Geology* **2014**, *171*, 59-69, doi:https://doi.org/10.1016/j.enggeo.2013.12.017.
10. Chen, J.; Dai, F.C.; Xu, L.; Chen, S.; Wang, P.F.; Long, W.; Shen, N.Q. Properties and microstructure of a natural slip zone in loose deposits of red beds, southwestern China. *Engineering Geology* **2014**, *183*, 53-64, doi:https://doi.org/10.1016/j.enggeo.2014.10.004.
11. Wang, J.; Cao, Y.C.; Liu, K.Y.; Costanzo, A.; Feely, M. Diagenesis and evolution of the lower Eocene red-bed sandstone reservoirs in the Dongying Depression, China. *Marine Petroleum Geology* **2018**, *94*, 230-245, doi:https://doi.org/10.1016/j.marpetgeo.2018.04.011.
12. Fan, C.F.; Teng, H.H. Surface behavior of gypsum during dissolution. *Chemical Geology* **2007**, *245*, 242-253, doi:https://doi.org/10.1016/j.chemgeo.2007.08.007.
13. Xin, L.; Xiyong, W.; Baolong, Z.; Jun, F. Study on the characteristics of black strata geochemical weathering and its disaster-causing mechanism. *Disaster Advances* **2012**, *5*, 1558-1562.
14. Li, A.R.; Deng, H.; Zhang, H.J.; Liu, H.H.; Jiang, M.L. The shear-creep behavior of the weak interlayer mudstone in a red-bed soft rock in acidic environments and its modeling with an improved Burgers model. *Mechanics of Time-Dependent Materials* **2023**, *27*, 1-18, doi:https://doi.org/10.1007/s11043-021-09523-y.
15. Zhou, Z.Q.; Song, H.Z. Elucidating the Manifestation of Subsurface Water Quality Components in Simulated Water-Rock Interactions. *Advancements in Hydraulic and Hydroelectric Science and Technology* **2001**, *21*, 17-20.
16. Mao, X.M.; Liu, X.; Barry, D.A. Application of PHREEQC on solute reactive transport modeling in groundwater. *Hydrogeology Engineering Geology* **2004**, *31*, 20-24.
17. He, J.; Niu, F.; Luo, F.; Jiang, H.; He, P.; Ju, X. Mechanical properties and modified binary–medium constitutive model for red–bed soft rock subjected to freeze–thaw cycles. *Cold Regions Science Technology* **2023**, *209*, 103803.

18. Zhou, C.Y.; Cui, G.J.; Yin, H.; Yu, L.; Xu, G.K.; Liu, Z.; Zhang, L.H. Study of soil expansion characteristics in rainfall-induced red-bed shallow landslides: Microscopic and macroscopic perspectives. *Plos one* **2021**, *16*, e0246214, doi:https://doi.org/10.1371/journal.pone.0246214.
19. Yu, W.D.; Liang, W.G.; Yu, Y.; Yang, X.Q. Micro-structure Development Research of Gypsum Salt Rock Soaked in Different Concentrations of Brine at Normal Temperature. *Journal of Taiyuan University of Technology* **2013**, *44*, 470-474.
20. Tiruta-Barna, L. Using PHREEQC for modelling and simulation of dynamic leaching tests and scenarios. *Journal of Hazardous Materials* **2008**, *157*, 525-533, doi:https://doi.org/10.1016/j.jhazmat.2008.01.028.
21. Marsac, R.; Davranche, M.; Gruau, G.; Bouhnik-Le Coz, M.; Dia, A. An improved description of the interactions between rare earth elements and humic acids by modeling: PHREEQC-Model VI coupling. *Geochimica et Cosmochimica Acta* **2011**, *75*, 5625-5637, doi:https://doi.org/10.1016/j.gca.2011.07.009.
22. Kim, S.S.; Baik, M.H.; Kang, K.C.; Kwon, S.H.; Choi, J.W. Solubilities of actinides in a domestic groundwater and a bentonite porewater calculated by using PHREEQC. *Journal of Industrial Engineering Chemistry* **2008**, *14*, 739-746.
23. Lipson, D.S.; Mccray, J.E.; Thyne, G.D. Using PHREEQC to Simulate Solute Transport in Fractured Bedrock. *Ground Water* **2010**, *45*, doi:https://doi.org/10.1111/j.1745-6584.2007.00318.x.
24. Zhang, C.C.; Bai, Q.S.; Han, P.H.; Wang, L.; Wang, X.; Wang, F.T. Strength weakening and its micromechanism in water–rock interaction, a short review in laboratory tests. *International Journal of Coal Science & Technology* **2023**, *10*, 10, doi:https://doi.org/10.1007/s40789-023-00569-6.
25. Meng, M.M.; Ge, H.K.; Shen, Y.H.; Ji, W.M.; Wang, Q.Y. Rock fabric of tight sandstone and its influence on irreducible water saturation in Eastern Ordos Basin. *Energy Fuels* **2023**, *37*, 3685-3696, doi:https://doi.org/10.1021/acs.energyfuels.2c04011.
26. Stuyfzand, P.J. An accurate, relatively simple calculation of the saturation index of calcite for fresh to salt water. *Journal of Hydrology* **1989**, *105*, 95-107, doi:https://doi.org/10.1016/0022-1694(89)90098-X.
27. Mac Nally, R.; Lake, P.S. On the generation of diversity in archipelagos: a re-evaluation of the Quinn-Harrison 'saturation index'. *Journal of Biogeography* **1999**, *26*, 285-295, doi:https://doi.org/10.1046/j.1365-2699.1999.00268.x.
28. Guo, Z.J.; Song, H.Z. Chemial Components in Ground Water and Its Sivalues. *Resources Environment and Engineering* **2005**, *19*, 200-202.
29. Zhang, S.; Xu, Q.; Hu, Z.M. Effects of rainwater softening on red mudstone of deep-seated landslide, Southwest China. *Engineering Geology* **2016**, *204*, 1-13.
30. Christopher, F.H.; Patil, S.R. Identification and review of sensitivity analysis methods. *Risk analysis* **2002**, *22*, 553-578.
31. Saltelli, A. Sensitivity analysis for importance assessment. *Risk analysis* **2002**, *22*, 579-590, doi:https://doi.org/10.1111/0272-4332.00040.
32. Potra, C.; Adrian, S.; florian, A. Sensitivity analysis for atmospheric chemistry models via automatic differentiation. *Atmospheric Environment* **1997**, doi:https://doi.org/10.1016/S1352-2310(96)00168-9.
33. Huang, K.; Cai, G.J.; Yan, C.; Yu, J.H.; Tang, L.P.; Zhang, J. Strength and microstructure characteristics of red-bed weathered residual soil stabilized by Titanium Gypsum-Cement. *Construction Building Materials* **2023**, *403*, 133071, doi:https://doi.org/10.1016/j.conbuildmat.2023.133071.
34. Wang, Z.Z.; Xu, M. Characteristics of red bed containing saline deposit and engineering geological issues of dam foundation in Sichuan basin *Water Resources and Hydropower Engineering* **2011**, *42(3)*, 10-12.
35. Wang, Y.S.; Wu, J.F.; Wei, P.; al., e. Research on time effect of rock weakening by water-rock interaction of red beds in Sichuan basin. *Chinese Journal of Rock Mechanics and Engineering* **2009**, *28(Supp.1)*, 3102-3108.
36. Wu, D.X.; Liu, H.J.; Wang, G.Q. Laboratory exoerimental study of slaking characteristics of red-bed soft rock. *Chinese Journal of Rock Mechanics and Engineering* **2010**, *29(Supp.2)* 4173-4179.
37. Zhang, B.X. A review of the application of hydrogeochemical methods in groundwater research. *Yellow River* **2019**, *41*.

38. Luo, J.; Jiang, Y.J.; Li, L.L.; Li, H.H.; Zheng, J.; Wu, J.F. Study on Environmental Susceptibility to Hydrochemical Variations in the Epikarst Spring. **2013**, 148-154.
39. Saltelli, A.; Ratto, M.; Tarantola, S.; Campolongo, F. Sensitivity Analysis for Chemical Models. *Chemical Reviews* **2005**, *105*, 2811-2828, doi:https://doi.org/10.1021/cr040659d.
40. Rabitz, H.; Kramer, M.; Dacol, D. Sensitivity Analysis in Chemical Kinetics. *Annual Review of Physical Chemistry* **1983**, *34*, 419-461, doi:10.1146/annurev.pc.34.100183.002223.
41. Seferlis, P.; Hrymak, A.N. Sensitivity analysis for chemical process optimization. *Computers Chemical Engineering* **1996**, *20*, 1177-1200, doi:https://doi.org/10.1016/0098-1354(96)82074-6.
42. He, J.L.; Niu, F.J.; Luo, F.; Jiang, H.Q.; He, P.F.; Ju, X. Mechanical properties and modified binary–medium constitutive model for red–bed soft rock subjected to freeze–thaw cycles. *Cold Regions Science and Technology* **2023**, *209*, 103803, doi:https://doi.org/10.1016/j.coldregions.2023.103803.
43. Leng, Y.Y.; Kong, X.Z.; He, J.Y.; Xing, A.G.; Zhang, Y.B.; Wang, Q. The July 10, 2020, red-bed landslide triggered by continuous rainfall in Qianxi, Guizhou, China. *Landslides* **2022**, *19*, 1421-1433, doi:https://doi.org/10.1007/s10346-022-01851-5.
44. El-Feky, M.S.; Kohail, M.; El-Tair, A.M.; Serag, M.I. Effect of microwave curing as compared with conventional regimes on the performance of alkali activated slag pastes. *Construction Building Materials* **2020**, *233*, 117268, doi:https://doi.org/10.1016/j.conbuildmat.2019.117268.
45. Xu, G.L.; Li, W.N.; Yu, Z.; Ma, X.H.; Yu, Z.Z. The 2 September 2014 Shanshucao landslide, Three Gorges Reservoir, China. *Landslides* **2015**, *12*, 1169-1178, doi:10.1007/s10346-015-0652-8.
46. Wang, T.; Gao, R.C.; Yan, C.Z. Dynamic fragmentation and chip formation of water-soaked rock in linear cutting with a coupled moisture migration-fracture model. *Computers and Geotechnics* **2023**, *163*, 105723, doi:https://doi.org/10.1016/j.compgeo.2023.105723.

Disclaimer/Publisher's Note: The statements, opinions and data contained in all publications are solely those of the individual author(s) and contributor(s) and not of MDPI and/or the editor(s). MDPI and/or the editor(s) disclaim responsibility for any injury to people or property resulting from any ideas, methods, instructions or products referred to in the content.

review 1

ORIGINALITY REPORT

23%	20%	20%	11%
SIMILARITY INDEX	INTERNET SOURCES	PUBLICATIONS	STUDENT PAPERS

PRIMARY SOURCES

1	Submitted to Kazakh-British Technical University Student Paper	2%
2	www.mdpi.com Internet Source	2%
3	www.preprints.org Internet Source	1%
4	Submitted to University of Nottingham Student Paper	1%
5	cyberleninka.org Internet Source	1%
6	Xiaomei Wang, Fan Deng, Haijian Cheng, Shuzheng Ning, Baoqing Li, Sidong Pan, Xuebo Yin. "Effects of Heating on the Binding of Rare Earth Elements to Humic Acids", Energies, 2022 Publication	1%
7	Elok Surya Pratiwi, Su-Min Shen, Junun Sartohadi. "Progress and challenges in designing landslide maps for disaster risk	1%

communication: a systematic review", Cartography and Geographic Information Science, 2023
Publication

8	minerva-access.unimelb.edu.au Internet Source	1 %
9	Jiawei Tan, Jingming Cai, Linchong Huang, Qiuning Yang, Mingjie Mao, Jiabin Li. "Feasibility of using microwave curing to enhance the compressive strength of mixed recycled aggregate powder based geopolymer", Construction and Building Materials, 2020 Publication	1 %
10	researchprofiles.canberra.edu.au Internet Source	1 %
11	www2.scut.edu.cn Internet Source	1 %
12	Marcelino Antonio Zúñiga-Estrada, Gabriela A. Vázquez-Rodríguez, Màrius Ramírez-Cardona, Liliana Lizárraga-Mendiola. "Mineralogical evidence of unfavorable geochemical interactions between urban runoff pollutants and filter materials in low-impact systems", Journal of Hazardous Materials, 2020 Publication	1 %

13	Yong Liu, Yanbin Yao, Dameng Liu, Chi Zhang. "Nuclear Magnetic Resonance Investigation of Forced Imbibitions in Longmaxi Shales: Consideration of Different Boundary Conditions", Energy & Fuels, 2023 Publication	1 %
14	Changdong Li, Zhiyong Fu, Ying Wang, Huiming Tang, Junfeng Yan, Wenping Gong, Wenmin Yao, Robert E. Criss. "Susceptibility of reservoir-induced landslides and strategies for increasing the slope stability in the Three Gorges Reservoir Area: Zigui Basin as an example", Engineering Geology, 2019 Publication	<1 %
15	assets.researchsquare.com Internet Source	<1 %
16	qjegh.lyellcollection.org Internet Source	<1 %
17	Yuchen Zheng, Chengzeng Yan, Hong Zheng. "Modified joint element constitutive model for FDEM to simulate the nonlinear mechanical behavior of rocks", Computers and Geotechnics, 2023 Publication	<1 %
18	cer.ihtm.bg.ac.rs Internet Source	<1 %
	matbio.org	

19	Internet Source	<1%
20	Submitted to University College London Student Paper	<1%
21	"Engineering Geology for Society and Territory - Volume 2", Springer Nature, 2015 Publication	<1%
22	www.cfdlab.ae.utexas.edu Internet Source	<1%
23	Xiansong Yin, Xiaojie Luo, Sanding Zhang, Jian Gao. "Formation setting and karst development characteristics of red beds in Wuhan, Hubei Province, China", IOP Conference Series: Earth and Environmental Science, 2020 Publication	<1%
24	research.unl.pt Internet Source	<1%
25	dspace.aus.edu:8443 Internet Source	<1%
26	researchspace.ukzn.ac.za Internet Source	<1%
27	www.nature.com Internet Source	<1%
28	core.ac.uk Internet Source	

		<1 %
29	repository.tudelft.nl Internet Source	<1 %
30	res.mdpi.com Internet Source	<1 %
31	Submitted to Agricultural Research Council Student Paper	<1 %
32	Dey, Arjun, and Anoop K. Mukhopadhyay. "In Vitro Dissolution, Microstructural and Mechanical Characterizations of Microplasma-Sprayed Hydroxyapatite Coating", International Journal of Applied Ceramic Technology, 2013. Publication	<1 %
33	Kai Huang, Guojun Cai, Chao Yan, Jinhuang Yu, Liping Tang, Jun Zhang. "Strength and microstructure characteristics of red-bed weathered residual soil stabilized by Titanium Gypsum-Cement", Construction and Building Materials, 2023 Publication	<1 %
34	jglobal.jst.go.jp Internet Source	<1 %
35	journals.rifst.ac.ir Internet Source	<1 %

36	Submitted to Korea Advanced Institute of Science and Technology Student Paper	<1 %
37	ouci.dntb.gov.ua Internet Source	<1 %
38	www.researchgate.net Internet Source	<1 %
39	Francesca Pianosi, Thorsten Wagener. "Distribution-based sensitivity analysis from a generic input-output sample", Environmental Modelling & Software, 2018 Publication	<1 %
40	www.disasterjournal.net Internet Source	<1 %
41	mdpi-res.com Internet Source	<1 %
42	Miyazaki, T., H. Yashiro, A. Nishikawa, and T. Tonozuka. "The side chain of a glycosylated asparagine residue is important for the stability of isopullulanase", Journal of Biochemistry, 2014. Publication	<1 %
43	Wei Hu, Gianvito Scaringi, Qiang Xu, Theo W.J. Van Asch, Runqiu Huang, Wenxi Han. "Suction and rate-dependent behaviour of a shear-zone soil from a landslide in a gently-inclined	<1 %

mudstone-sandstone sequence in the Sichuan basin, China", Engineering Geology, 2018
Publication

44	Renneng Bi, Dominik Ehret, Wei Xiang, Joachim Rohn, Markus Schleier, Jiwei Jiang. "Landslide reliability analysis based on transfer coefficient method: A case study from Three Gorges Reservoir", Journal of Earth Science, 2012 Publication	<1 %
45	Liangxuan Yan, Quanbing Gong, Fei Wang, Lixia Chen, Deying Li, Kunlong Yin. "Integrated Methodology for Potential Landslide Identification in Highly Vegetation-Covered Areas", Remote Sensing, 2023 Publication	<1 %
46	Maikol Solís. "Non-parametric estimation of the first-order Sobol indices with bootstrap bandwidth", Communications in Statistics - Simulation and Computation, 2019 Publication	<1 %
47	www.dza.de Internet Source	<1 %
48	www.micromagazine.com Internet Source	<1 %
49	www.netl.doe.gov Internet Source	<1 %

50	Submitted to South Bank University Student Paper	<1%
51	Xin Liao, Qi Xu, Sixiang Ling, Angran Tian, Qiang Tang. "Degradation Characteristics and Mechanism of Black Sandy Dolomite with Fluid Added in a Mechanical Test", Geofluids, 2023 Publication	<1%
52	link.springer.com Internet Source	<1%
53	Jiapei Du, Annan Zhou, Xiaoshan Lin, Yuhuan Bu, Jayantha Kodikara. "Revealing Expansion Mechanism of Cement-Stabilized Expansive Soil with Different Interlayer Cations through Molecular Dynamics Simulations", The Journal of Physical Chemistry C, 2020 Publication	<1%
54	Lixiao Hou, Liqiang Ma, Kewang Cao, Naseer Muhammad Khan, Xiujuan Feng, Zhitao Zhang, Anye Cao, Dangliang Wang, Xuebin Wang. "Analysis of fracture characteristics of saturated sandstone based on infrared radiation variance", Physics and Chemistry of the Earth, Parts A/B/C, 2024 Publication	<1%
55	businessdocbox.com Internet Source	<1%

56	publications.goettingen-research-online.de Internet Source	<1 %
57	www.ijain.org Internet Source	<1 %
58	"Advancing Culture of Living with Landslides", Springer Science and Business Media LLC, 2017 Publication	<1 %
59	Bin Yu, Erlong Ma, Jiajun Cai, Qiang Xu, Weile Li, Guang Zheng. "A prediction model for rock planar slides with large displacement triggered by heavy rainfall in the Red bed area, Southwest, China", Landslides, 2020 Publication	<1 %
60	Kun He, Anmin Nie, Yifei Yuan, Seyed Mohammadreza Ghodsi et al. "In Situ Transmission Electron Microscopy Explores a New Nanoscale Pathway for Direct Gypsum Formation in Aqueous Solution", ACS Applied Nano Materials, 2018 Publication	<1 %
61	Nai Hao, Yongliang Wang, Hao Cheng, Xiaochong Wu, Yi Zhao. "Hydration Absorption and Thermal Effects of Outcrop Porous Sandstone Based on Intelligent Experimental and Infrared Thermography Techniques", Energies, 2023 Publication	<1 %

62	Roderick W. Kumimoto, Cory T. Ellison, Tania Y. Toruño, Aurélie Bak et al. "XAP5 CIRCADIAN TIMEKEEPER Affects Both DNA Damage Responses and Immune Signaling in Arabidopsis", Frontiers in Plant Science, 2021 Publication	<1 %
63	ebin.pub Internet Source	<1 %
64	scholarbank.nus.edu.sg Internet Source	<1 %
65	www.scirp.org Internet Source	<1 %
66	www.skb.com Internet Source	<1 %
67	Anrun Li, Hui Deng, Haojie Zhang, Hanhan Liu, Mingliang Jiang. "The shear-creep behavior of the weak interlayer mudstone in a red-bed soft rock in acidic environments and its modeling with an improved Burgers model", Mechanics of Time-Dependent Materials, 2021 Publication	<1 %
68	Qingyuan Liu, Peng Zhang, Bixin Cheng, Yong Li, Jia Li, Huhai Zhou, Gan Sun, Jie Qing, Zaixiang Zhu, Yun Lu, Pengxiao Zhao. "Incorporating the life stages of fish into	<1 %

habitat assessment frameworks: A case study in the Baihetan Reservoir", Journal of Environmental Management, 2021
Publication

---

69 Ebrahim Sharifi Teshnizi, Mehdi Mirzababaei, Jafar Karimiazar, Reza Arjmandzadeh, Kamran Mahmoudpardabad. "Gypsum and rice husk ash for sustainable stabilization of forest road subgrade", Quarterly Journal of Engineering Geology and Hydrogeology, 2023 <1 %
Publication

---

70 Haoqiang Lai, Cuiying Zhou, Zhen Liu. "Ecological membrane for slope engineering based on red bed soil", PLOS ONE, 2023 <1 %
Publication

---

71 Peng Mo, Qiongzhen Tang, Junhui Luo, Haifeng Huang, Qing Yang, Yu Chen. "Study on time-effect to the strength deterioration of carbonaceous mudstone under water-rock interaction", Matéria (Rio de Janeiro), 2023 <1 %
Publication

---

72 thesesups.ups-tlse.fr <1 %
Internet Source

Exclude quotes	Off	Exclude matches	Off
Exclude bibliography	On		